J Mol Model (2016) 22: 51
DOI 10.1007/s00894-016-2916-1

ORIGINAL PAPER

A two-layer ONIOM study of thiophene cracking catalyzed by proton- and cation-exchanged FAU zeolite

Yingxin Sun[1] · **Xinfeng Mao**[1] · **Supeng Pei**[1]

Received: 3 September 2015 / Accepted: 18 January 2016 / Published online: 3 February 2016

Abstract A two-layer ONIOM study on the hydrodesulfurization mechanism of thiophene in H-FAU and M-FAU (M = Li^+, Na^+, and K^+) has been carried out. The calculated results reveal that in H-FAU, for a unimolecular mechanism, the rate-determining step is hydrogenation of alkoxide intermediate. The assistance of H_2O and H_2S molecules does not reduce the difficulty of the C-S bond cracking step more effectively. A bimolecular hydrodesulfurization mechanism is more favorable due to the lower activation barriers. The rate-determining step is the formation of 2-methylthiophene, not the C-S bond cracking of thiophene. Moreover, the ring opening of thiophene is much easier to occur than the desulfurization step. A careful analysis of energetics indicates that H_2S, propene, and methyl thiophene are the major products for the hydrodesulfurization process of thiophene over H-FAU zeolite, in good agreement with experimental findings. In M-FAU zeolites, both unimolecular and bimolecular cracking processes are difficult to occur because of the high energy barriers. Compared to the case on H-FAU, the metal cations on M-FAU increase the difficulty of occurrence of bimolecular polymerization and subsequent C-S bond cracking steps.

Keywords Thiophene · Hydrodesulfurization mechanism · Cation-exchanged FAU zeolite · C-S bond cracking · Bimolecular desulfurization step

Introduction

Thiophene, benzothiophene, and their alkyl derivatives represent a large fraction of the total organosulfur compounds in fluidized catalytic cracking (FCC) gasoline. Sulfur in gasoline causes toxic emissions and inefficient activity of automobile catalytic converters; thus, their removal techniques have attracted increased attention [1, 2]. Hydrotreatment of FCC feed, hydrodesulfurization (HDS), and selective adsorption desulfurization are the main strategies for this. High costs are involved in the hydrotreatment process. The conventional HDS catalysts consist of metal sulfides such as Ni-Mo or W-Ni dispersed into a γ-Al or zeolite support [3]. The disadvantage of the HDS process is an H_2 atmosphere, often at high pressures, which tends to saturate high-octane alkene and arene components in gasoline and thus lead to a significant loss of octane number. Although a selective adsorption technique avoids these drawbacks, the low adsorption capacities and selectivities of materials limited its applications [4].

Interestingly, many experimental studies have suggested that acidic zeolites alone also can catalyze HDS [5]. Zeolites are microporous crystalline solids with well-characterized nanopores, high specific area, and good thermal stabilities, which make them potential catalysts for the removal of sulfur compounds. For example, Chica et al. measured the adsorption dynamics and stoichiometry of thiophene and its derivatives in different carriers on H-ZSM5 and H-FAU zeolites [6]. They found that H-FAU showed higher adsorption uptakes and that oligomerization could occur on acid sites. Moreover, C_3H_8 carrier removed a larger fraction of

Electronic supplementary material The online version of this article (doi:10.1007/s00894-016-2916-1) contains supplementary material, which is available to authorized users.

✉ Yingxin Sun
sunyingxin0312@sit.edu.cn

✉ Supeng Pei
peisupeng@126.com

[1] School of Chemical and Environmental Engineering, Shanghai Institute of Technology, Shanghai, China

thiophene-derived intermediates than H_2 and so hydrogen atoms formed during propane dehydrogenation reactions. Richardeau et al. investigated the adsorption and reaction of thiophene over H-FAU zeolites in liquid hydrocarbon solutions [7]. They concluded that thiophene removal by adsorption over acidic zeolites could only be performed from diluted solutions containing no olefins. Shan et al. reported that thiophenic species could crack over USY zeolite to produce propene, butene, and H_2S [8]. Valla et al. revealed that heavy aromatic sulfur compounds such as 4,6-dimethyldibenzothiophene and benzothiophene are stable species and difficult to desulfurize, which do not affect the percentage of sulfur in gasoline [9]. The long-chain alkylated thiophenic derivatives are responsible for the fraction of sulfur content. Although previous experimental studies proposed several cracking mechanisms of thiophene species [6, 8], these reaction pathways are not enough to understand the overall elementary steps in detail from a theoretical standpoint. More importantly, whether there exists any competitive relationship between different reactions steps is still vague.

Actually, in the case of the HDS reactions, the alkali or transition metal cations are often used to enhance the reaction rates. Angelis et al. investigated the infrared spectra of thiophene adsorbed over Na-FAU, 13X, and H-FAU zeolites [10]. Their infrared spectrum data indicated the cleavage of thiophene C-S bond and the formation of -SH groups on H-FAU zeolite. Welters et al. studied the influence of zeolite acidity on thiophene HDS activity for H(x)/Na-FAU-supported metal sulfide catalysts [11]. The results showed that the acidic supports themselves could also desulfurize thiophene at reaction conditions. Yu et al. reported that on H-ZSM5, Zn/H-ZSM5, and Co/H-ZSM5 with propane as the exclusive hydrogen source, the presence of Zn^{2+} and Co^{2+} cations increased desulfurization rates [12]. Propane dehydrogenation could be coupled with thiophene hydrogenation to improve thiophene desulfurization selectivities. Similarly, Garcia and Lercher studied adsorption and surface reactions of thiophene on Na-, K-, and H-ZSM5 by IR spectroscopy [13]. They concluded that in the cation-exchanged samples, a strong coordinative bonding formed between thiophene and Na^+ and K^+ cations. The ring opening and oligomerization reactions occurred by the strong acidity of the H-ZSM5. Simon et al. carried out a thiophene TPD study on acidic, alkali-exchanged, and Pt-supported MOR and LTL zeolites [14]. The increase of the alkali content of the zeolites improved the fraction of thiophene that desorbed without decomposing. The decomposition of thiophene is mainly due to the Brønsted acid sites. In particular, recent studies have shown that Ag^+ and Cu^+ cation-exchanged Y zeolites exhibited superior adsorption selectivities for thiophenic species [15]. In addition to the adsorption process, the role of metal cations in HDS mechanisms on cation-exchanged zeolites is interesting but remains unclear.

Despite the great progress made over the past few decades in experimental fields, a systematic atomic-level study is urgently required to understand the complicated desulfurization process of thiophene. Several key theoretical progresses have been made. In 1999, Saintigny et al. performed a density functional theory (DFT) study of the desulfurization of thiophene using a 3-T cluster model ($H_3SiOHAl(OH)_2OSiH_3$) to represent acidic zeolite [16]. Two different mechanisms occurring with and without the participation of hydrogen, have been compared. Rozanska et al. carried out DFT calculations using a 4-T zeolitic cluster [17]. They concluded that the acidity of zeolite was not a key factor and even methyl alkoxide or Li-exchanged zeolite could also catalyze cracking reactions of thiophene. Subsequently, Rozanska et al. performed a periodic DFT study on the C-S bond cracking mechanisms of thiophenic derivatives on proton- or Li-exchanged MOR zeolite [18]. The calculated results showed that the zeolite framework could not stabilize the transition state (TS) complexes mainly due to zwitterionic nature of the TS structures. Recently, Li et al. proposed a new bimolecular mechanism of thiophene C-S bond-cracking on acidic ZSM5 zeolite and pointed out that the rate-determining step is the electrophilic aromatic substitution [19]. Their results were in good accord with the experiments. Summarizing the above-mentioned theoretical studies, two main methods have been widely used to investigate the reactions of HDS process: the bare cluster model and the periodic DFT method. For the former, it is difficult to understand the effect of the zeolite framework. The periodic DFT method is straightforward but very computationally demanding if large zeolite crystal cells are involved. A recently developed quantum mechanical/molecular mechanical (QM/MM) method as well as the more general ONIOM (Our-own-N-layered Integrated molecular Orbital + molecular Mechanics) scheme have been extensively used to study mechanisms of chemical reactions [20–22]. This scheme is employed in this article because it combines the advantages of the high accuracy of quantum chemistry and the high efficiency of molecular mechanics force fields.

Herein, we performed a two-layer ONIOM study on the HDS mechanism of thiophene in proton- and cation-exchanged FAU zeolites (i.e., H-FAU and M-FAU (M = Li^+, Na^+, and K^+), respectively). For comparison, the alkyl derivative of thiophene, 2-methylthiophene, has also been investigated. Our objective is to address the following three interesting questions. (1) What are the elementary steps involved in the complete catalytic cycle for the HDS process? (2) How are the products such as H_2S, propene, and methyl thiophene produced, and what is the rate-determining step? (3) What is the role of metal cations in the HDS process? The elucidation of the reactions mechanisms provides insights into the fundamental steps of the reactions, which should prove useful for optimizing the reaction conditions and designing new catalysts for industrial production.

Computational details

The extended 156 T nanocluster, covering the active region of the H-FAU zeolite, was used to represent the Brønsted acid site and the zeolite framework in this work. The atomic coordinates of this model were taken from crystal structure for the H-FAU cell with cubic *Fd-3 m* space group ($a = b = c = 24.258$ Å, $\alpha = \beta = \gamma = 90.0°$) [23]. Figure 1 illustrates the 156 T model, which covers two supercages connected to each other through the 12-membered-ring (12MR) window. The Brønsted acid site is represented by colored balls. An Si atom is substituted by an Al atom, and a proton is attached to the bridging oxygen atom bonded directly to the Al atom. This oxygen atom is conventionally called the O1 position. In this model, the dangling bonds of the Si atoms were terminated by H atoms and the Si-H bonds were fixed at 1.47 Å along the Si-O bonds of the FAU framework.

According to the two-layer ONIOM approach, the computation model is divided into two regions, and the total ONIOM energy of the whole system is expressed as

$$E_{\mathrm{ONIOM2}} = E_{\mathrm{MM}}^{\mathrm{All}} - E_{\mathrm{MM}}^{\mathrm{Inner}} + E_{\mathrm{QM}}^{\mathrm{Inner}} \quad (1)$$

where the subscript "All" region includes an inner region (i.e., the active Brønsted acidic site and reacting species) calculated with a high-level quantum mechanics (QM) approach and a large outer region (i.e., the extended zeolite framework) treated only with a less expensive molecular mechanics (MM) level [24]. Both QM and MM calculations need to be carried out for the "inner" system. In this approach, the classical van der Waals (VDW) and long-range electrostatic contributions were evaluated by the MM calculations.

The difference of MM calculations between the whole system and inner system, the *S*-value, describes the contribution from the MM region [25].

$$S^{\mathrm{MM}} = E_{\mathrm{MM}}^{\mathrm{All}} - E_{\mathrm{MM}}^{\mathrm{Inner}} \quad (2)$$

The *S*-value is part of total ONIOM energy and must be continuous in potential energy surface. For a given transition state structure, this continuity must be independent of the definition of the TS connectivity whether as in the reactant structure or the product structure in the reaction center, i.e.,

$$\Delta S^{\mathrm{MM}} = S^{\mathrm{MM}}(\mathrm{TS,\ reaction\ connectivity}) - S^{\mathrm{MM}}(\mathrm{TS,\ product\ connectivity}) = 0 \quad (3)$$

An *S*-value test can check whether the partitioning scheme of the whole ONIOM system is correct. We chose several representative transition states of the HDS process on H-FAU and M-FAU zeolites and found that all the calculated ΔS^{MM} values were zero (see Table S1 of the Supporting Information, SI).

The DFT using the M06-2X hybrid meta-GGA functional [26] and the universal force field (UFF) [27] were used as default to describe the inner and outer regions, respectively. According to previous work reported by Zhao et al., the well-known B3LYP functional systematically underestimates barrier heights for a collection of 76 energy barriers of hydrogen-transfer and non-hydrogen-transfer reactions and thus not enough to treat medium-range VDW interactions [28]. The newly developed density functional, M06-2X, could be considered to recover the dispersion interactions as reliably as the MP2 method with the benefit of feasible computational costs. In the ONIOM calculations, we divided the inner region into two subregions and employed mixed basis sets. A 12-T subregion including the acidic site of zeolite and reacting molecules was described using the 6-31G(d,p) basis set; the other 6-T subregion of the inner region was described using the 3-

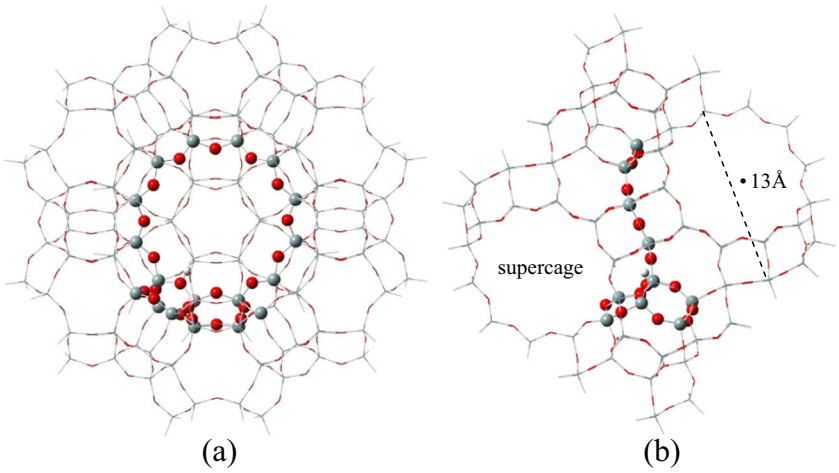

Fig. 1 156T nanocluster model of H-FAU zeolite divided into two regions, the inner 18 T region (*colored balls*) is computed with the quantum mechanics method and the outer region (*lines*) computed with UFF: front view (**a**) and side view (**b**) (colored balls: *gray*, silicon; *red*, oxygen; *pink*, aluminum; *white*, hydrogen)

21G basis set. This combination rule was called M06-2X(12 T(6-31G(d,p)):6 T(3-21G)). The mixed basis sets were employed in order to save computational time. Correspondingly, the whole zeolite model was called ONIOM(M06-2X(12 T(6-31G(d,p)):6 T(3-21G)):UFF) or ONIOM(18 T:156 T). The ONIOM model of 18 T/156 T cluster of H-FAU is considered to be reliable enough for investigating the HDS reaction mechanism in the bulk catalytic systems due to a large number of previous theoretical studies [29, 30]. During the structure optimizations, only the 5-T region [(≡SiO)$_3$Al(OH)Si≡] and reacting species were allowed to relax, while the rest of the 156-T model was fixed along the crystallographic coordinates. The frequency calculations were performed at the same level of theory to ensure that each stationary point exhibited the proper number of imaginary frequencies: none for an intermediate and exactly one for a transition state (the first-order saddle point). To obtain more reliable interaction energies, the single-point energy calculations at the M06-2X(12 T(6-311 + G(2df,2p)): 6 T(6-31G(d,p))) and MP2(12 T(6-311 + G(d,p)):6 T(6-31G(d,p))) levels were carried out for the QM regions using the previously optimized geometries produced by the M06-2X functional. The single-point-energy scheme at the MP2 level was denoted MP2//M06-2X. The final ONIOM(MP2//M06-2X:UFF) energy values were referred to when energies were discussed, unless specifically noted. The single-point energy data at the M06-2X(12 T(6-311 + G(2df,2p)):6 T(6-31G(d,p))) level were given in SI (Tables S4–S6) because all the conclusions obtained from Tables S4–S6 are almost the same as those from MP2//M06-2X energy data.

An important feature in zeolite catalysis is the stabilization of cation-like transition state structures by the zeolite framework. The long-range electrostatic contributions in the MM calculations are crucial to describe the interactions between cation-like transition states and anion-like zeolite fragments. However, the charge parameters in the UFF force field were not optimized to represent the electrostatic potentials (ESP) in zeolites [27]. To solve this problem, we calculated the ESP energy of a 116-T pure silica zeolite model by M06-2X/6-31G(d,p) energy calculations. The atomic charge parameters for the MM region were obtained by fitting the ESP energy using a constrained-fit scheme. In the QM region, the atomic charge values for each reacting molecule were taken directly from the ESP charges produced by the DFT calculations with M06-2X functional using the ChelpG scheme [31]. Charge neutrality constraint was imposed for the whole system, i.e., both QM and MM regions have no net charge, the same as the whole system. The mechanical embedding scheme was used for evaluating the electrostatic interactions between QM and MM regions, which has been applied successfully to catalytic mechanism investigations [32, 33]. All the calculations in the present study were performed using the Gaussian 09 program [34].

Results and discussion

Based on the previous experimental and theoretical work [6, 8, 19], we have proposed the reaction mechanisms of HDS process of thiophene molecules over H-FAU and M-FAU zeolites by locating the related intermediates and transition states of the elementary steps. The proposed pathways are summarized in Schemes 1, 2, 3, and 4 and the corresponding energy profiles are given in Figs. 2 and S1–S3. It should be mentioned that according to the previously reported result by Li et al., the α site of thiophene molecule is more reactive than β site or sulfur center [19]. Therefore, in the bimolecular mechanism (Scheme 3), we focus our attention on the formation of C_α-C_α bond between two thiophene molecules. All energy values are given as the following rule. For each intermediate or transition state, energy data are calculated relative to the total energy of the reactant molecule (thiophene) and the zeolite (H-FAU or M-FAU) at infinitive separation. For each transition state, the corresponding activation barrier can be obtained as energy difference between the transition state and its previous intermediate.

In H-FAU zeolite, the HDS process of thiophene may proceed through unimolecular mechanism to produce 1-butene and H_2S or bimolecular mechanism to produce propene, 2-methylthiophene, and H_2S. The main product, such as propene, 2-methylthiophene, and H_2S, are in good accord with experimental observations over H-FAU. In pure M-FAU zeolite, cracking of the C-S bond of thiophene molecule can occur via both unimolecular and bimolecular mechanisms but no H_2S is produced. The detailed reaction pathways are discussed in the following sections as reported in Schemes 1, 2, 3, and 4 and Figs. 2 and S1–S3.

Unimolecular cracking mechanism of thiophene in H-FAU zeolite

The capture of thiophene by the acid site of zeolite is the first step to initiate the HDS reaction. Three different types of adsorption modes, η^1(S), η^2(CC), and η^1(C), are obtained, with the adsorption energies of -110.76, -108.10, and -112.59 kJ/mol, respectively. The BSSE [35] corrected adsorption energies are -57.48, -54.22, and -52.33 kJ/mol, respectively. The η^1(S) adsorption mode is slightly more favorable than others, which is in accord with previous experimental observations in H-FAU [36].

The geometrical parameters of adsorbed thiophene, complex-TH-1, are shown in Fig. 3. For the η^1(S) adsorption mode, the thiophene interacts with the solid-acid proton from zeolite through a S…H bond distance of 2.36 Å. The O1-H distance of H-FAU is lengthened by 0.01 Å compared with that in the pure H-FAU. In the η^2(CC) adsorption mode, there is an interaction between acidic proton and C_α=C_β bond of thiophene with H-C_α and H-C_β distances of 2.08 and 2.22 Å,

Scheme 1 The proposed unimolecular mechanism of HDS process for thiophene in H-FAU zeolite

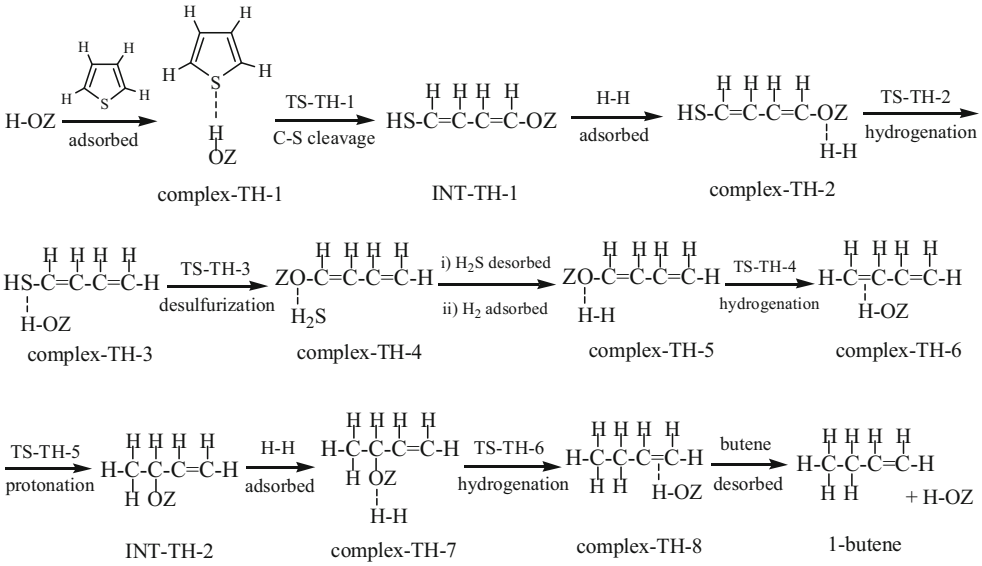

respectively. In the η^1(C) mode, the thiophene is adsorbed to acidic proton of zeolite with a H-C_β distance of 2.10 Å. For the latter two adsorption modes, the O1-H distance is lengthened by 0.02 Å.

After adsorption of thiophene on the acidic site of zeolite, thiophenic ring cracking will proceed through a protonation step. The acidic hydrogen protonates the sulfur atom and the activation energy is 357.36 kJ/mol (Fig. 2), indicating that the C-S bond cracking process is experimentally disfavored. Using the cluster approach method, Rozanska et al. reported that the activation energy for thiophene cracking is 226 kJ/mol [17]. Moreover, they performed a periodic DFT study and found that the activation energy for C-S cracking of thiophene catalyzed by H-MOR zeolite is 318 kJ/mol [18]. Our calculated result is accord with their reported values. The optimized structure of transition state TS-TH-1 is shown in Fig. S4. It can be seen that in TS-TH-1, the acidic proton H is getting close to the sulfur atom, the C-S bond of thiophene is breaking and ring is opening, and simultaneously the new C-O bond is forming. The involved OH…S, C-S, and C-O bond distances are 1.98, 2.60, and 1.80 Å, respectively.

Thiophene cracking leads to the formation of an alkoxy species, INT-TH-1. Then, a H_2 molecule is co-adsorbed with INT-TH-1 near the active site of zeolite (complex-TH-2 in Fig. S4) and then reacts with INT-TH-1 through a transition state TS-TH-2 of hydrogenation step to produce complex-TH-3 (Scheme 1). The calculated activation energy of hydrogenation step is 251.58 kJ/mol, which is consistent with the previously theoretical values (about 215 kJ/mol) reported by Saintigny et al. using DFT method with a 3 T cluster model [16]. In complex-TH-3 as given in Fig. S5, there is a typical H-bonding for sulfur atom interacting with the acidic proton from zeolite with a distance of 2.29 Å, which facilitates subsequent desulfurization process. In TS-TH-3, the acidic proton has been captured by sulfur atoms. The breaking C-S bond is 2.35 Å and the forming C-O bond is 2.02 Å. This

Scheme 2 The proposed mechanism of HDS process for 2-methylthiophene in H-FAU zeolite

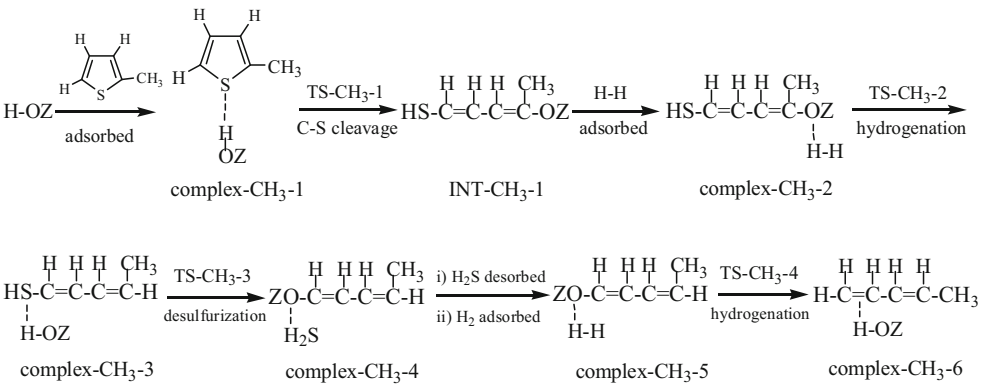

Scheme 3 The proposed bimolecular mechanism of HDS process for thiophene in H-FAU zeolite

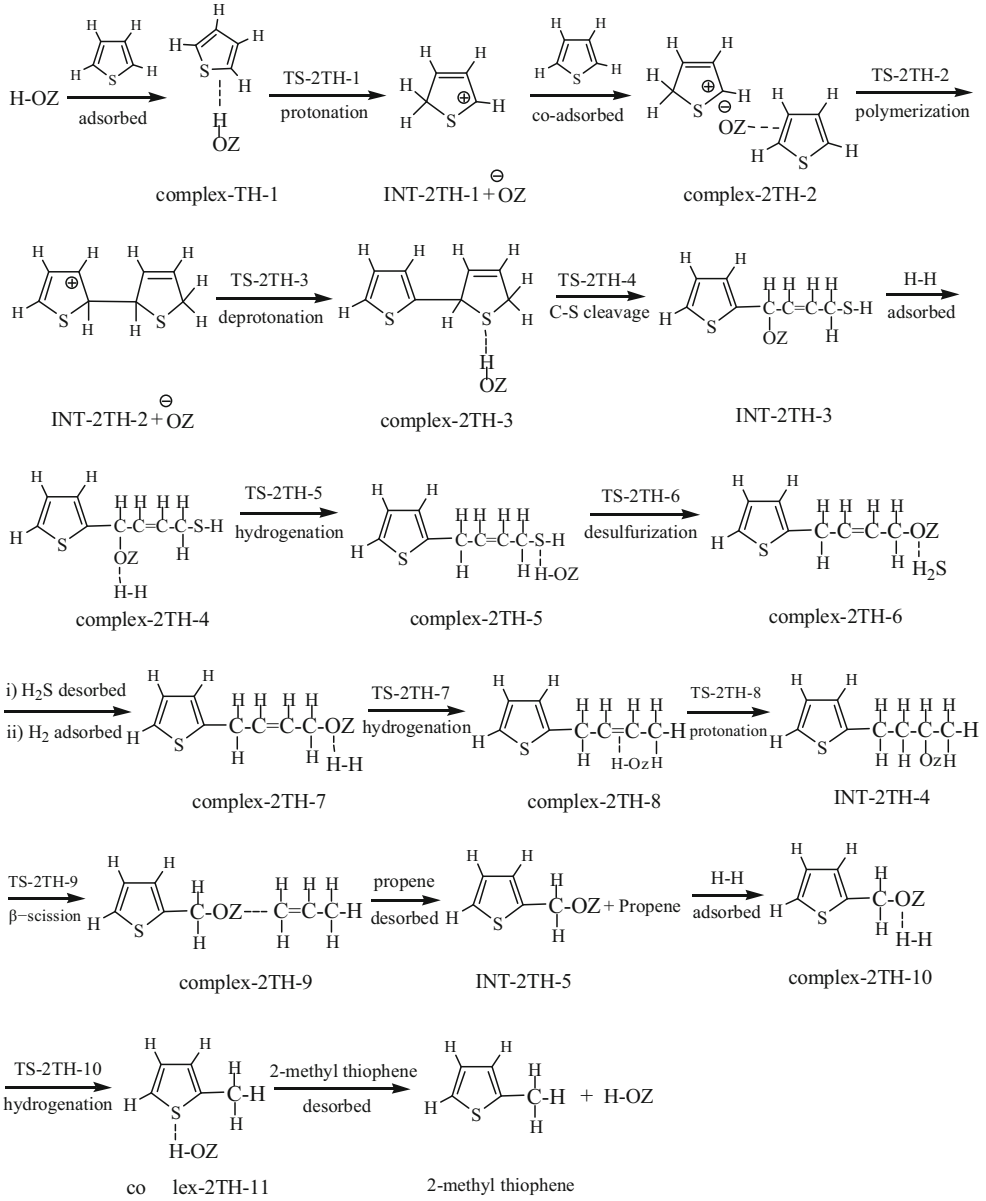

desulfurization step needs to overcome an activation energy of 278.44 kJ/mol. After the TS, the H_2S molecule is produced and an alkoxide intermediate is formed with a C-O bond distance of 1.44 Å, as given in complex-TH-4 (see Fig. S5).

After the desorption of H_2S from the complex-TH-4, a H_2 molecule is adsorbed in complex-TH-5, followed by hydrogenation of alkoxide intermediate with an activation energy of 264.31 kJ/mol (Fig. 2). The corresponding structure and energy barrier of transition state TS-TH-4 (Fig. S6) are similar to those of TS-TH-2 (Fig. S5). The H-H distance of H_2 molecule is lengthened from 0.74 Å in complex-TH-5 to 0.85 Å in TS-TH-4. The hydrogenation step yields the 1,3-butadiene molecule as shown in Scheme 1. Through protonation and hydrogenation steps, the 1,3-butadiene could be finally converted into 1-butene. The involved transition states TS-TH-5 and TS-TH-6 are given in Fig. S6.

Now we investigate the rate-determining step for the unimolecular cracking mechanism. According to the study reported by Murdoch [37], the rate-determining step of a multistep reaction can be found by dividing the whole reaction sequence into several different sections. Each section begins with an intermediate and terminates with another intermediate, which is more stable than the previous intermediate. One should compute the energy difference between the transition state with the highest energy and the initial intermediate in each section and the largest energy difference will contain the rate-determining step. In present work, from Fig. 2, three sections, complex-TH-1 to complex-TH-6, complex-TH-6 to complex-TH-7, and complex-TH-7 to complex-TH-8, are

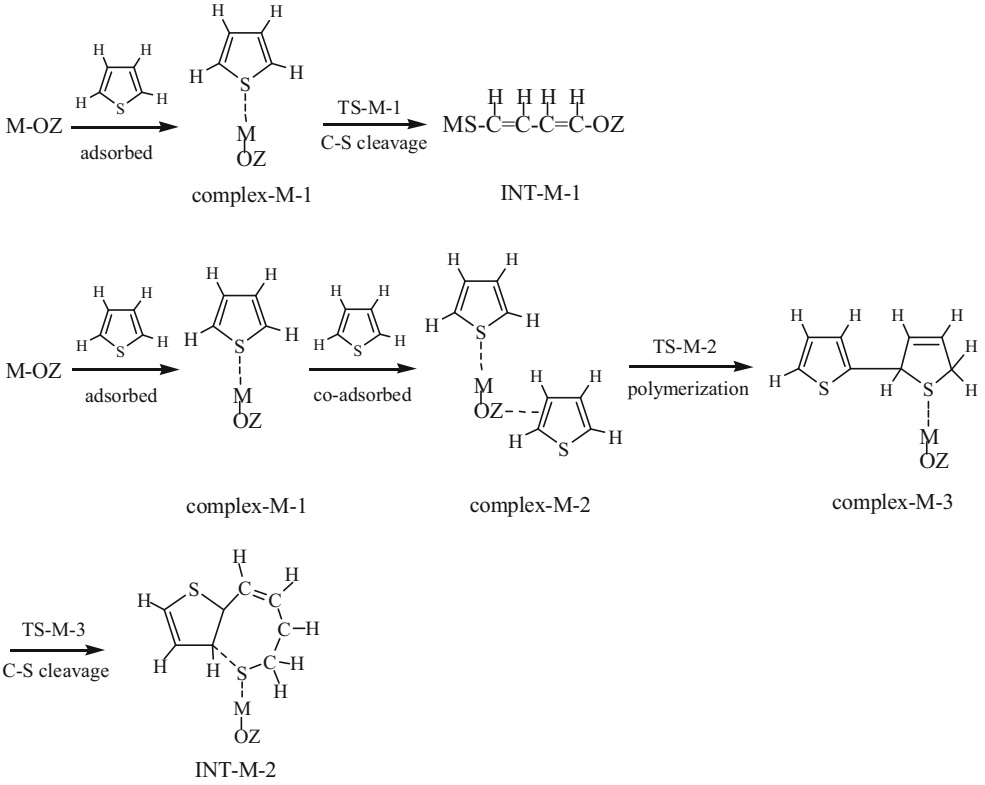

Scheme 4 The proposed mechanism of cracking process for thiophene in M-FAU zeolite (M = Li^+, Na^+, and K^+)

involved. It can be seen that the largest energy difference is obtained in the first section (from complex-TH-1 to complex-TH-6), which contains the transition state, TS-TH-2 with the highest energy. The corresponding overall energy barrier is calculated to be 432.97 kJ/mol relative to the complex-TH-1. Therefore, the rate-determining step for the unimolecular cracking mechanism should be hydrogenation of INT-TH-1 via TS-TH-2, rather than the desulfurization step (TS-TH-3) and C-S bond cracking of thiophene (TS-TH-1), although the activation barrier of C-S bond cracking step (TS-TH-1) is largest in all of the individual steps. We analyzed the activation barriers of all six steps in terms of QM and MM components, as given in Table S2. Clearly, the MM energies are small and thus the stability of transition states is mainly due to the QM contributions.

According to our previous theoretical studies, the 1-butene could be catalyzed by H-ZSM5 and H-FAU zeolites to produce propene and ethene via direct cracking and dimerization cracking mechanisms [38]. So the reaction mechanisms on the formation of propene and ethene will not be discussed in this work. Chica et al. experimentally investigated the effects of zeolite structure and Al content on thiophene adsorption, desorption, and surface reactions on H-ZSM5, H-Beta, and H-FAU zeolites. They found that propene is one of the major products in the HDS process over H-FAU [6]. Our result is also in accord with experimental observations.

Hydrogen sulfide (H_2S) is one of the main products of desulfurization process of thiophenic species. Water molecules are the common components in the air. The presence of H_2O can lead to a deactivation of the active sites and at high temperature to the destruction of the Brønsted sites. Rozanska et al. reported that H_2O and H_2S can serve as assistant molecules in reducing the activation energy of C-S bond cracking step, using the DFT method and a small zeolitic cluster model [17]. In this work, we investigated the performance of their assistance behaviors and obtained the optimized transition state structures, TS-TH-1-H_2O and TS-TH-1-H_2S, as shown in Fig. S7. In TS-TH-1-H_2O, the acidic proton is attacking the O atom of water molecule. One hydrogen atom in H_2O is closer to the sulfur atom of thiophene molecule, which finally leads to the C-S bond cracking and formation of new C-O bond. The configuration of TS-TH-1-H_2S is similar to that of TS-TH-1-H_2O. The main difference between them is that the degree of protonation of water molecule by acidic proton in TS-TH-1-H_2O is larger than that of H_2S in TS-TH-1-H_2S, which can be seen from the geometrical parameters in Fig. S7. Interestingly, the calculated activation energies are 351.54 and 385.36 kJ/mol for the above-reported H_2O- and H_2S-assisting transitions states, respectively, significantly higher than the theoretical values (202 and 219 kJ/mol, respectively) [17] of Rozanska et al. A comparison of activation energies for C-S bond cracking step with and without assistant molecules clearly suggests that the presence of H_2O can slightly reduce the difficulty of the thiophenic ring-opening process, but on the contrary, H_2S can increase the difficulty greatly. This viewpoint is partially different from

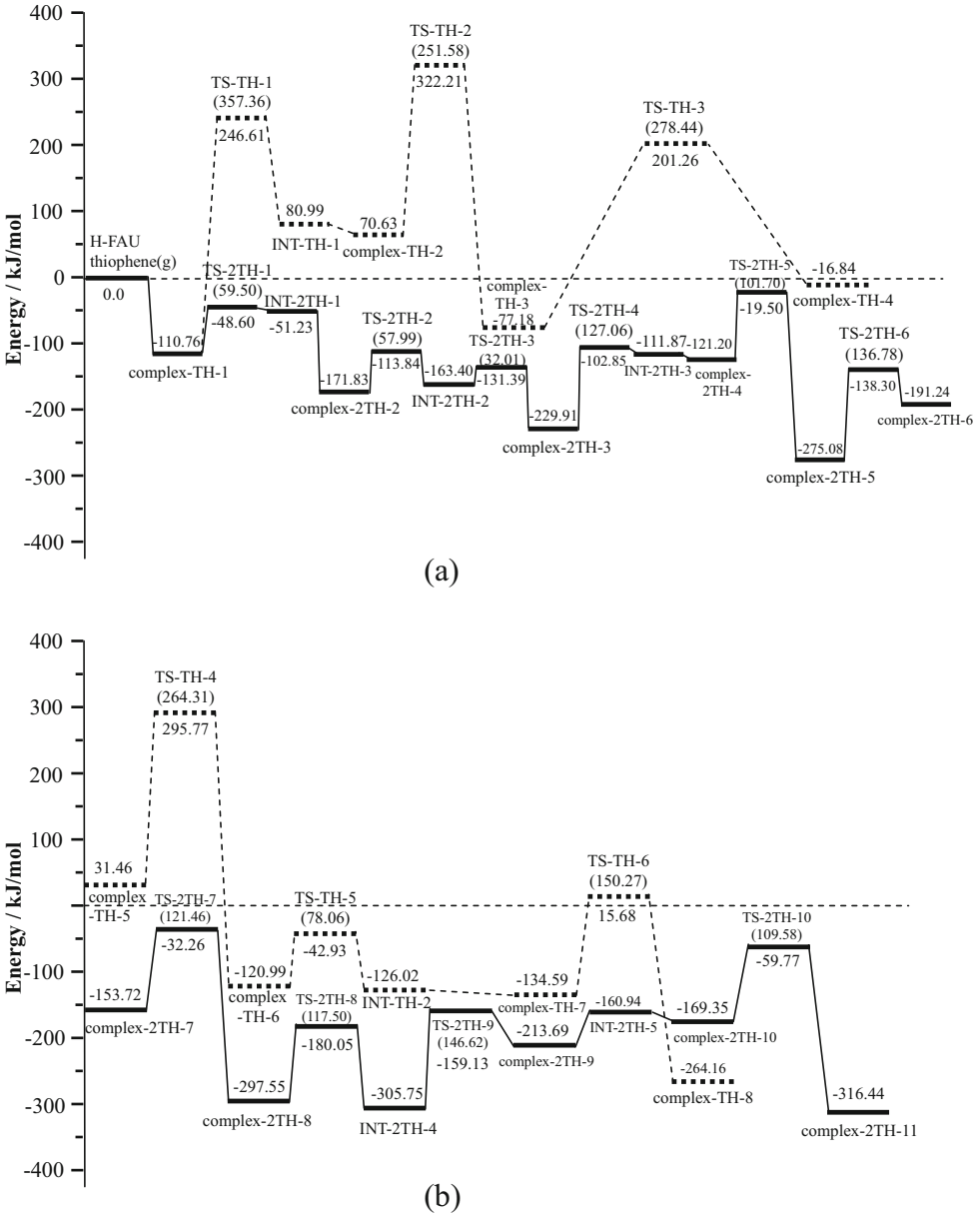

Fig. 2 Energy profiles calculated for unimolecular (*dashed lines*) and bimolecular (*solid lines*) HDS reaction pathways over H-FAU illustrated in Schemes 1 and 3. Energy data calculated for each species are relative to the total energy of the reactant (thiophene) and the H-FAU zeolite at infinitive separation. For transition states, activation barriers, ΔE_{act} are given in parentheses. The *x*-axis represents the reaction coordinate of HDS process

that of Rozanska et al. In the discussion below, the model involving assistant molecules will not be investigated.

Unimolecular cracking mechanism of 2-methylthiophene in H-FAU zeolite

To understand the influence of an electron-donating group on thiophene cracking process, we studied the unimolecular HDS mechanism of 2-methylthiophene in H-FAU zeolite as described in Scheme 2. The involved reaction pathway is overall similar to that of the thiophene molecule. The selected geometrical parameters of key intermediates and transition states are shown in Figs. S8 and S9.

Figure S8 shows three different adsorption modes of 2-methylthiophene over H-FAU, η^1(S), η^2(CC), and η^1(C), with BSSE corrected adsorption energies of -48.61, -64.76, and -64.74 kJ/mol, respectively. These adsorption configurations are similar to those of thiophene molecule. However, the most stable adsorption mode is not η^1(S), but η^2(CC), which is different from the thiophene case. In the η^2(CC), the acidic proton points towards the $C_\beta = C_\beta$ double bond of 2-methylthiophene with H-C_β distance of approximately 2.2 Å, while the methyl group interacts with zeolitic framework through weak hydrogen bonds.

The subsequent reaction step is the ring opening of 2-methylthiophene. From Scheme 2, it can be seen that the C-S bond of 2-methylthiophene is cleaved via transition state, TS-CH_3-1, to form alkoxide INT-CH_3-1. The cracking step of C-S bond needs to overcome an energy barrier of 342.73 kJ/mol, slightly lower than that in the thiophene case. One

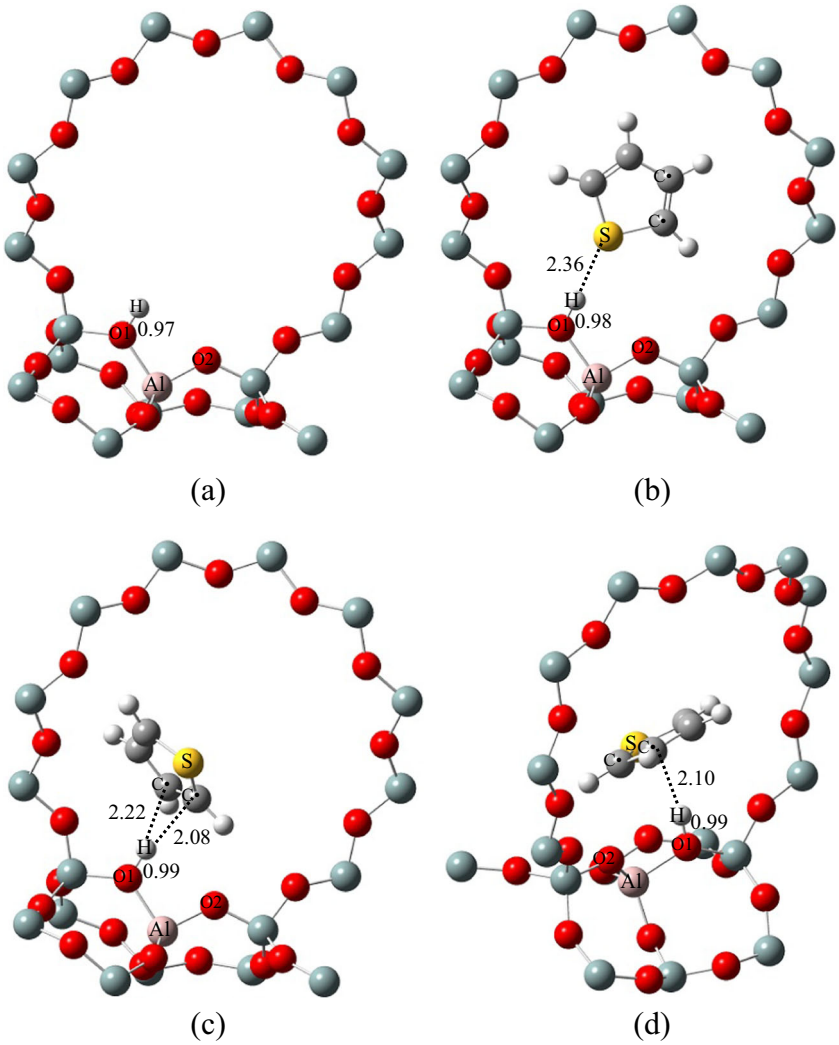

Fig. 3 Optimized structures of three different adsorption modes for thiophene adsorbed in H-FAU zeolite. **a** H-FAU, **b** η^1(S), **c** η^2(CC), and **d** η^1(C). Key distances are marked in units of Å

hydrogen molecule is then co-adsorbed with INT-CH_3-1, leading to the formation of complex-CH_3-2. The complex-CH_3-2 reacts through TS-CH_3-2 to yield complex-CH_3-3, followed by a desulfurization step with the activation energy of 294.87 kJ/mol for TS-CH_3-3. As compared to that of thiophene, the desulfurization process of 2-methylthiophene is slightly more difficult. From the resulting complex-CH_3-4, H_2S is desorbed and simultaneously H_2 is co-adsorbed to form complex-CH_3-5. Finally, 1,3-pentadiene molecule is yielded from complex-CH_3-5 through a hydrogenation step (TS-CH_3-4). According to previously published studies [39–41], the complicated reaction networks, involving such as protonation, dimerization, and hydrogenation, can take place from olefin molecules such as 1,3-pentadiene catalyzed by the acidic zeolites. Investigating these reaction steps is not our objective because the sulfur content has been removed in the above-mentioned mechanisms.

Figure S1 gives the energy profile calculated for unimolecular HDS reaction pathways of 2-methylthiophene over H-FAU illustrated in Scheme 2. According to the study reported by Murdoch [37], only one section, complex-CH_3-1 to complex-CH_3-6, is involved because only complex-CH_3-6 is lower in energy than the first intermediate, complex-CH_3-1. So the rate-determining step should be the hydrogenation of complex-CH_3-5 via TS-CH_3-4 of highest energy in this section, although the activation barrier of C-S bond cracking step (TS-CH_3-1) is largest in all of the individual steps (see Fig. S1).

The involved structural parameters of four transition states, TS-CH_3-1 to TS-CH_3-4, are given in Fig. S9. As compared to the unimolecular cracking mechanism of thiophene, the difference of transition state structures is small. For example, the TS-CH_3-1 structure resembles that of TS-TH-1 (see Fig. S4(a)). Also, in both TS-TH-3 and TS-CH_3-3, the H_2S molecule is almost completely formed. As expected, the similar geometrical structures give rise to similar energetics. For instance, the C-S bond cracking steps of thiophene and 2-methylthiophene need to overcome activation barriers of 357.36 and 342.73 kJ/mol, respectively. The energy difference of two activation barriers is less than 15 kJ/mol. For the

desulfurization step, the corresponding energy difference is still very small, less than 17 kJ/mol, suggesting the weak and limited influence of electron-donating $-CH_3$ group on unimolecular HDS process of thiophene.

Bimolecular cracking mechanism of thiophene in H-FAU zeolite

The bimolecular cracking mechanism is a newly emerging alternative for the unimolecular mechanism of thiophene, which is proposed by Shan [8], Aksenov [42], and Chica et al. [6, 43]. As described in Scheme 3, five main steps are involved: (1) protonation of thiophene in the channel of H-FAU zeolite, (2) dimerization of two thiophene molecules, (3) C-S bond cracking and ring opening of the dimerized thiophene molecule, (4) removal of sulfur content, and (5) β-scission of carbon chain to produce propene molecule, together with several other steps such as hydrogenation and protonation. A more detailed discussion will be given below.

First, the adsorbed thiophene molecule (complex-TH-1, η^2(CC) mode in Fig. 3) is protonated to form the INT-2TH-1 through transition state, TS-2TH-1 (Fig. 4a), with the activation barrier of 59.50 kJ/mol. Then, the second thiophene is co-adsorbed on the first protonated thiophene (complex-2TH-2 in Fig. 4c). Subsequently, the complex-2TH-2 undergoes an electrophilic aromatic substitution step to produce the intermediate INT-2TH-2. The corresponding transition state is TS-2TH-2 (Fig. 4d) and needs to overcome an activation barrier of 57.99 kJ/mol. The resulting INT-2TH-2 can be deprotonated through TS-2TH-3 (Fig. 5b) with an activation barrier of 32.01 kJ/mol and complex-2TH-3 is produced. Interestingly, it should be mentioned that Li et al. reported that in H-ZSM5 zeolite, the complex-2TH-3 could be formed by a concerted dimerization step of two thiophene molecules with an energy barrier of 101 kJ/mol [19, 44]. Our calculations suggested that the formation of complex-2TH-3 should occur through a stepwise pathway. At the TS-2TH-1, the thiophene is almost protonated with the C_α-H bond length of 1.21 Å. In the TS-2TH-2, the distance between the two bonding carbon atoms ($C_\alpha - C_\alpha$) is 1.99 Å. After the TS-2TH-3, the Brønsted acid site is restored, enabling further catalytic reactions.

The next step is the C-S bond cracking of complex-2TH-3 through a transition state TS-2TH-4. At the TS-2TH-4 presented in Fig. 5d, the C-S bond is elongated to 3.15 Å. The corresponding activation barrier is calculated to be 127.06 kJ/mol, higher than the result of Li et al. using a 56 T ZSM5 cluster (66.1 kJ/mol) [19], highlighting the importance of different topological structures of zeolites. Also, this energy barrier is obviously lower than that of unimolecular C-S bond breaking step of thiophene mentioned above (357.36 kJ/mol), indicating that this cracking process should occur preferably via bimolecular mechanism.

After TS-2TH-4, the INT-2TH-3 is produced, and then proceeds through a hydrogenation reaction with activation barrier of 101.70 kJ/mol for TS-2TH-5 (Fig. 6a). The resulting complex-2TH-5 reacts to remove the sulfur atom via transition state TS-2TH-6. In TS-2TH-6 (Fig. 6b), the breaking C-S bond and forming C-O bond are 2.60 and 2.23 Å, respectively. Interestingly, this step needs to only overcome 136.78 kJ/mol, greatly lower than that of unimolecular desulfurization (278.44 kJ/mol). Our calculated value is also lower than the result of Saintigny et al. (167 kJ/mol) using a bare cluster model [16], implying the importance of zeolite environments.

Subsequently, the H_2S is desorbed from complex-2TH-6 and one H_2 molecule adsorbed to form complex-2TH-7 (Scheme 3). Two subsequent steps, hydrogenation and protonation, take place with activation barriers of 121.46 (TS-2TH-7) and 117.50 kJ/mol (TS-2TH-8), respectively (Fig. 2), producing the intermediate INT-2TH-4. Herein, propene is yielded from INT-2TH-4 through a β-scission reaction (TS-2TH-9). This step needs to overcome a moderate energy barrier of 146.62 kJ/mol, which suggests that the formation of propene may occur under industrial HDS conditions (363–773 K) [43]. The geometrical parameters of INT-2TH-4 and TS-2TH-9 are given in Fig. 6. In TS-2TH-9, one propene molecule is almost completely produced. After the desorption of propene, the INT-2TH-5 reacts with H_2 molecule via a hydrogenation step to yield 2-methylthiophene with a small activation barrier of 109.58 kJ/mol (TS-2TH-10), and also, the acidic site is finally restored. Table 1 presents the energy decompositions in QM and MM contributions for all reaction steps. Again, the stabilities of transition states are mainly due to the QM contributions.

A careful investigation from Table 1 suggests that the ring opening of thiophene (127.06 kJ/mol) is much easier to occur than the desulfurization step (136.78 kJ/mol). The H_2 molecule is necessary for completing the hydrogenation reactions. One can readily find that the occurrence of the hydrogenation step needs lower activation barriers in the bimolecular HDS mechanism (smaller than about 120 kJ/mol, Table 1) but higher in unimolecular mechanism (larger than 150 kJ/mol, Table S2), probably attributed to the influence of the second thiophene ring in the dimerized thiophene species. It is also noteworthy that Zecchina et al. confirmed the formation of oligomeric thiophene species in H-FAU zeolite by means of IR and UV-Vis spectra [45]. In the current work, the polymerization reaction of two thiophene molecules occurs easily due to the low activation barrier (57.99 kJ/mol), in accord with their experimental observations.

Figure 2 gives the energy profiles calculated for unimolecular and bimolecular HDS reaction pathways over H-FAU illustrated in Schemes 1 and 3. According to the study reported by Murdoch [37], six sections in the bimolecular pathway are involved: complex-TH-1 to complex-2TH-2, complex-2TH-2 to complex-2TH-3, complex-2TH-3 to

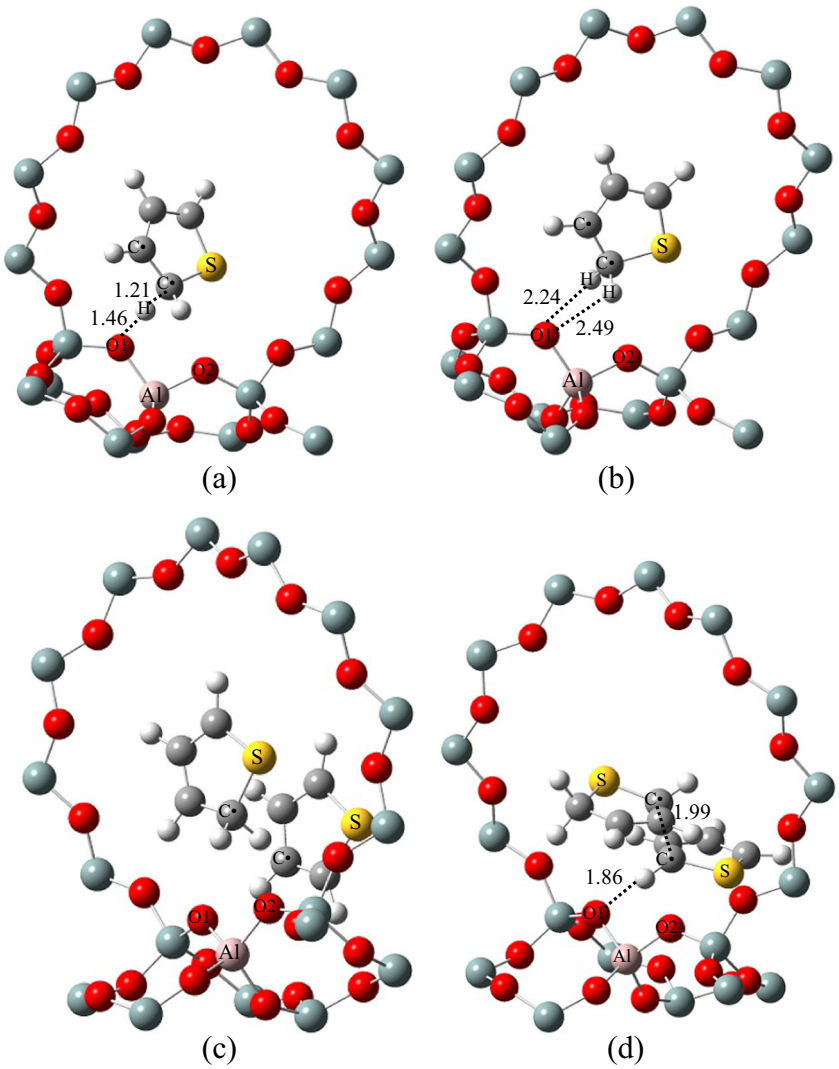

Fig. 4 Optimized structures of **a** TS-2TH-1, **b** INT-2TH-1, **c** complex-2TH-2, and **d** TS-2TH-2 in H-FAU zeolite for bimolecular cracking mechanism of thiophene. Key distances are marked in units of Å

complex-2TH-5, complex-2TH-5 to complex-2TH-8, complex-2TH-8 to INT-2TH-4, and INT-2TH-4 to complex-2TH-11. The corresponding energy differences between transition state of highest energy and their respective initial intermediate for each section are calculated to be 59.50 (TS-2TH-1), 57.99 (TS-2TH-2), 210.41 (TS-2TH-5), 242.82 (TS-2TH-7), 117.50 (TS-2TH-8), and 245.98 kJ/mol (TS-2TH-10), respectively. So the formation of 2-methylthiophene via TS-2TH-10 in the last section should be the rate-determining step for the bimolecular cracking mechanism. An energy barrier of 109.58 kJ/mol is needed for the single step from complex-2TH-10 to TS-2TH-10. From the point of view of thermodynamics, one can see that from Fig. 2, all of the intermediates and transition states are lower in energy in PES relative to the initial reactants (thiophene and HFAU), which indicates that H_2S, propene, and methyl thiophene may be the thermodynamically favorable major products over H-FAU zeolite, despite several slightly high individual activation barriers such as desulfurization (136.78 kJ/mol) and β-scission (146.62 kJ/mol) steps. This result is in good agreement with the experimental findings in H-FAU reported by Chica and Jaimes et al. [6, 46, 47]. In addition, a comparison of unimolecular and bimolecular HDS mechanisms from Fig. 2 shows that the ring opening of thiophene and removal of sulfur content are more favorable through bimolecular mechanism.

It should be noted that we have obtained another transition state of desulfurization step of thiophene, as described in Fig. 7. In Scheme 1, the complex-TH-3 proceeds via TS-TH-3 to remove the sulfur atom. Instead, the complex-TH-3 can also be protonated to form INT-uni-concert, followed by a transition state, TS-TH-3-concert, for the removal of sulfur atom. The geometrical parameters of INT-uni-concert and TS-TH-3-concert are given in Fig. 7a and b, respectively. In TS-TH-3-concert, the –SH group on the terminal C1 atom and the H atom on the nearest-neighbor C2 atom leave the C1-C2 bond simultaneously to produce the H_2S molecule. Similarly, in the Scheme 3, the complex-2TH-4 (i.e., the INT-2TH-3 with one adsorbed H_2 molecule) reacts via TS-2TH-5 to yield

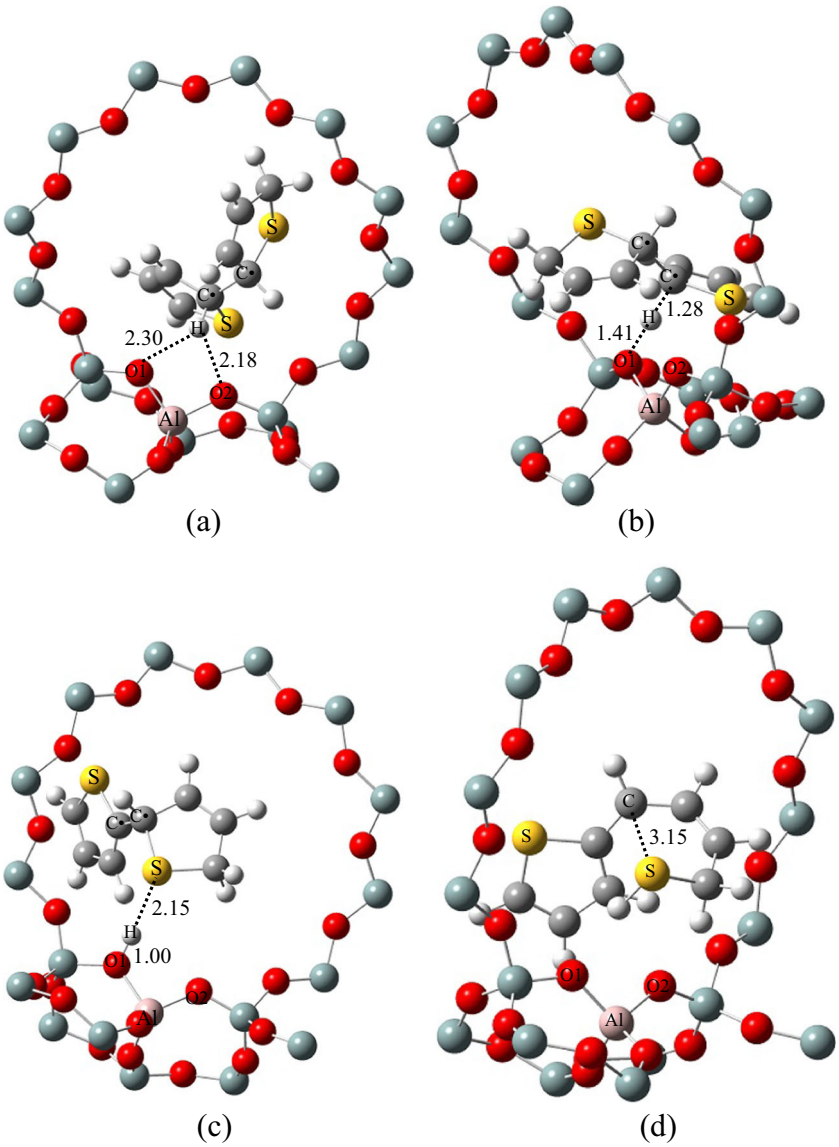

Fig. 5 Optimized structures of **a** INT-2TH-2, **b** TS-2TH-3, **c** complex-2TH-3, and **d** TS-2TH-4 in H-FAU zeolite for bimolecular cracking mechanism of thiophene. Key distances are marked in units of Å

complex-2TH-5, followed by TS-2TH-6 for the desulfurization step. Alternatively, the INT-2TH-3 can also be converted into INT-bi-concert (Fig. 7c). H_2S molecule can be desorbed directly from the INT-bi-concert through transition state TS-2TH-6-concert. As expected, the geometrical configurations of TS-TH-3-concert (Fig. 7b) and TS-2TH-6-concert (Fig. 7d) are similar to each other and their activation barriers are 330.83 and 326.27 kJ/mol, respectively. Such high energy barriers make the corresponding desulfurization steps quite difficult to occur practically.

Cracking mechanisms of thiophene in cation-exchanged FAU zeolite

In this section, the influence of metal cations such as Li^+, Na^+, and K^+ on the cracking mechanism of thiophene over FAU zeolite has been investigated. The participation of H_2 molecules will possibly lead to the formation of Brønsted acid sites. Furthermore, the presence of both acidic sites and metal cations will make the desulfurization mechanism of thiophene more complicated. For convenience, we only focus our attention on the cracking mechanism in the absence of H_2 molecules, as given in Scheme 4.

In the M-FAU, the metal cation can be located in different positions with different stabilities, whereas it is not our objective in current work. We only investigate the cases near the acidic sites and the behavior of inactive metal cations will not be studied. Figure S10 presents the structures of M-FAU. One can see that there are two weak bonds, M…O1 and M…O2, with almost equally bond lengths, which is consistent with the ESR experiment and previous theoretical study [30, 48]. The order of the distance of metal cation to acidic zeolite oxygen atoms O1 (or O2) is $Li^+ < Na^+ < K^+$, probably due to the different cation radius and different electronegativity.

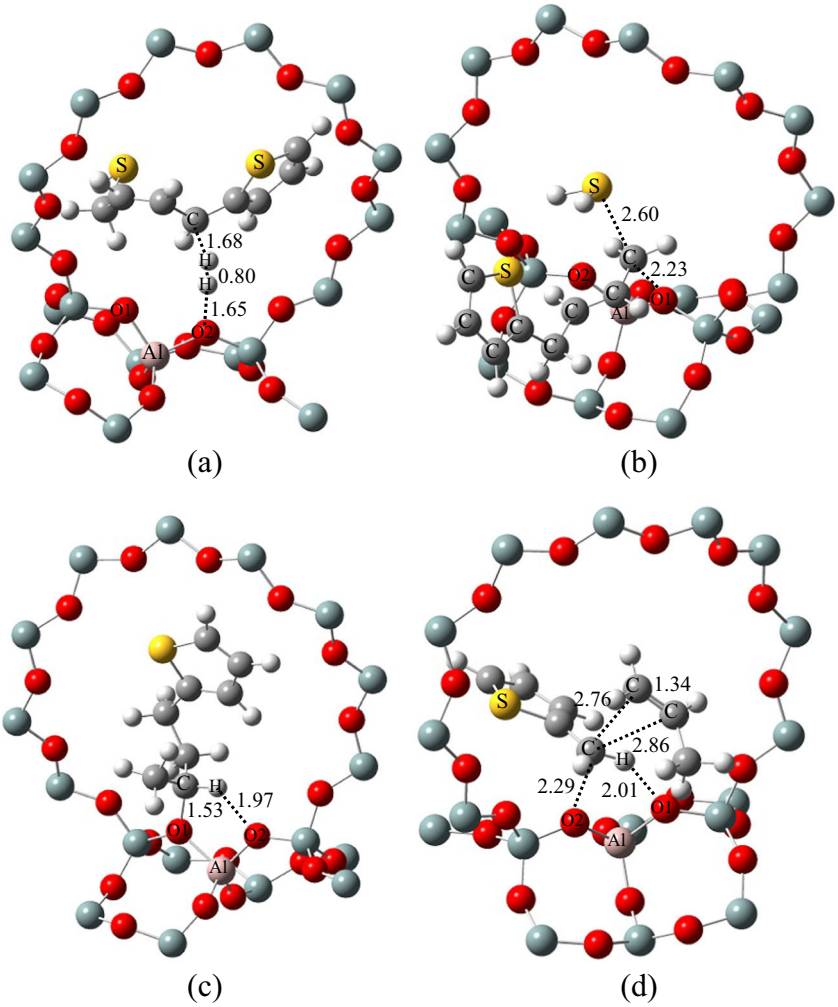

Fig. 6 Optimized structures of **a** TS-2TH-5, **b** TS-2TH-6, **c** INT-2TH-4, and **d** TS-2TH-9 in H-FAU zeolite for bimolecular cracking mechanism of thiophene. Key distances are marked in units of Å

Similar to the case of H-FAU, the thiophene is initially adsorbed on the M-FAU. For the Li-FAU, there are two types of adsorption modes, η^1(S) and η^5, as described in Fig. S11 (complex-Li-1). In the structure of η^1(S) mode, a weak Li…S bond is formed with a distance of 2.50 Å. For the η^5 mode, the Li^+ cation interacts with the thiophene ring. The distance from Li^+ to the center of the thiophene ring is 2.12 Å. For both Na-FAU and K-FAU zeolites, two adsorption modes, η^1(S) and η^2(CC), are obtained and their structural parameters are also given in Fig. S11. A careful comparison shows that the order of distance between metal cation and thiophene is $Li^+ < Na^+ < K^+$, which is the same order as for the distance of M…O1 (or M…O2) in M-FAU.

Table 1 Activation barriers (kJ/mol) of bimolecular mechanism of thiophene for all ten steps at the ONIOM(MP2//M06-2X:UFF) level and decompositions in QM and MM contributions

Species	Steps	QM	MM	ONIOM
TS-2TH-1	Protonation	61.38	−1.88	59.50
TS-2TH-2	Polymerization	59.17	−1.18	57.99
TS-2TH-3	Deprotonation	29.07	2.95	32.01
TS-2TH-4	C-S cracking	113.96	13.10	127.06
TS-2TH-5	Hydrogenation	115.70	−14.01	101.70
TS-2TH-6	Desulfurization	138.70	−1.93	136.78
TS-2TH-7	Hydrogenation	128.22	−6.76	121.46
TS-2TH-8	Protonation	121.18	−3.68	117.50
TS-2TH-9	β-scission	149.80	−3.17	146.62
TS-2TH-10	Hydrogenation	99.54	10.04	109.58

The shorter distance of metal cation to thiophene leads to the higher adsorption energy of thiophene. The most stable adsorption modes are η^5 in Li-FAU, η^2(CC) in Na-FAU, and η^2(CC) in K-FAU, with the BSSE corrected adsorption energies of -83.69, -67.44, and -55.39 kJ/mol, respectively. No experimental adsorption data are found for thiophene adsorbed in Li-FAU and K-FAU. Fortunately, Takahashi et al. reported that the heat of adsorption from experimental isotherms data in Na-FAU (Si/Al = 2.43) is - 79.91 kJ/mol (the lower limit) [49]. Our calculated result is lower than the experimental value probably because of the higher ratio of Si/Al (Si/

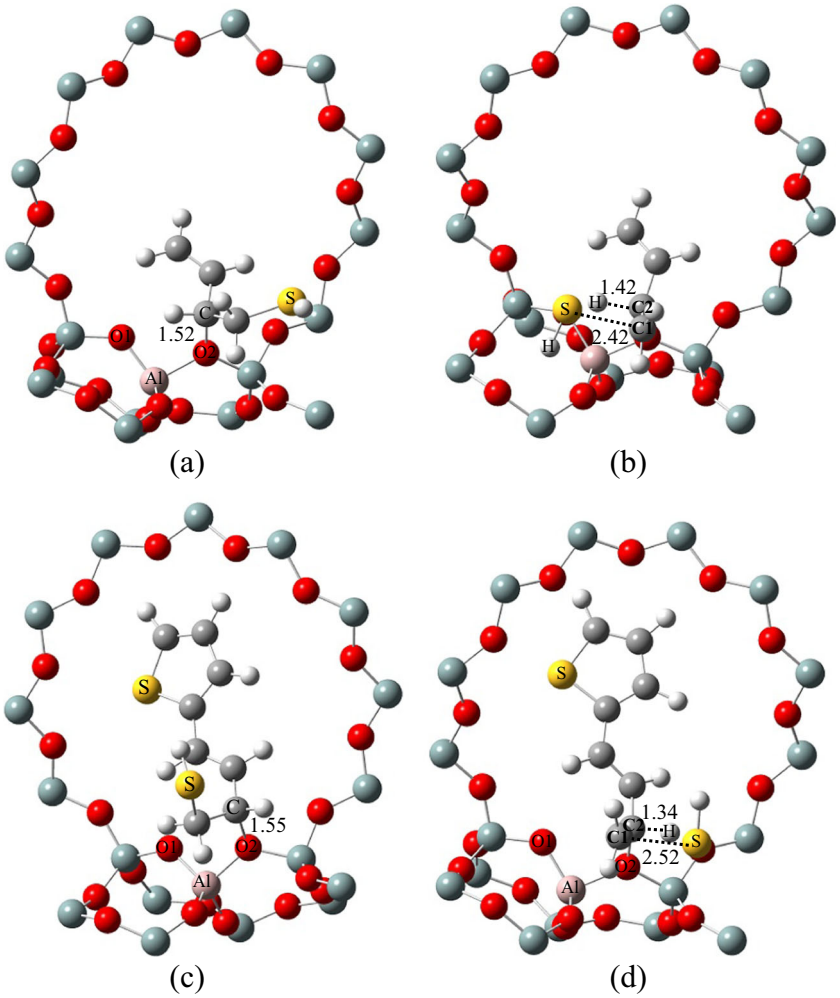

Fig. 7 Optimized structures of **a** INT-uni-concert, **b** TS-TH-3-concert, **c** INT-bi-concert, and **d** TS-2TH-6-concert in H-FAU zeolite for concerted desulfurization step of thiophene. Key distances are marked in units of Å

Al = 155) and thus the smaller number of metal cations in current zeolite models.

After complex-M-1, the C-S bond cracking occurs through transition state, TS-M-1, to form the intermediate, INT-M-1. At the TS-Li-1 in Fig. S12, the forming Li-S bond and breaking C-S bond distances are 2.43 and 2.57 Å, respectively. The configuration of TS-Li-1 is similar to those of TS-Na-1 and TS-K-1 (Fig. S12) with the activation barriers of 342.66, 338.30, and 394.92 kJ/mol, respectively, higher than theoretical DFT result (205 kJ/mol) using a bare 4 T Li-cluster reported by Rozanska et al.[17]. Compared to that of TS-TH-1 (357.36 kJ/mol) in H-FAU, one can conclude that the metal cations could not reduce the difficulty of the unimolecular C-S bond cracking step more effectively. Moreover, different from the case of H-FAU, the resulting INT-M-1 could not react to produce H_2S without the participation of H_2 molecules in M-FAU zeolites.

Scheme 4 presents the proposed mechanism of cracking process for thiophene in M-FAU. After one thiophene is adsorbed near the active site, the second thiophene molecule is co-adsorbed interacting with the zeolitic framework. The complex-M-2 subsequently proceeds through a transition state, TS-M-2, to form a complex-M-3. This polymerization step needs to overcome energy barriers of 248.28, 254.42, and 221.91 kJ/mol for TS-Li-2, TS-Na-2, and TS-K-2, respectively. The C-S bond cracking step of complex-M-3 takes place through TS-M-3 with the activation barriers of 243.78, 249.41, and 346.83 kJ/mol for $M = Li^+$, Na^+, and K^+, respectively. Obviously, the higher energy barriers of polymerization and C-S bond cracking steps relative to that in H-FAU (92.37 and 127.06 kJ/mol) suggests that the metal cations do not reduce and contrarily increase the difficulty of occurrence of these two steps. The resulting INT-M-2 could not complete the desulfurization process in the absence of H_2 molecules and no H_2S is produced. Furthermore, the calculated high activation barriers make the initial reactions unfavorable. Therefore, it can be seen that the removal of sulfur content is achieved essentially by means of physisorption of thiophene, not the chemical desulfurization process. This conclusion is in good agreement with the experimental observations of Simon et al., i.e., no H_2S is found for thiophene adsorption in Na-MOR and K-LTL zeolites [14].

The optimized geometrical parameters of complex-M-2, TS-M-2, complex-M-3, and TS-M-3, are given in Fig. S13 ($M=Li^+$) and Figs. S14 and S15 ($M=Na^+$ and K^+). We take the Li-FAU as an example. Interestingly, the configuration of TS-Li-2 is very different from TS-2TH-2 (Fig. 4d), leading to the different polymerization process. At TS-Li-2 in Fig. S13, the C_α atom of the first thiophene is attacking another C_α atom of the second thiophene. The forming C_α-C_α bond length is 1.73 Å. Simultaneously, the C_α-H bond of the first thiophene is breaking and the new C_α-H bond of the second thiophene is forming. The breaking and forming C_α-H bond distances are 1.23 and 1.75 Å, respectively. Different from the H-FAU case, the Li^+ cation does not participate in the concerted polymerization process directly and only stabilizes the transition state structure through a weak Li…S bond (2.56 Å). The Li^+ cation plays the same role in TS-Li-3 with a breaking C-S bond distance of 3.07 Å. For $M=Na^+$ and K^+, the geometrical configurations of transition states are more or less similar to the case for $M=Li^+$.

Several remarks can be obtained from the QM and MM energy components of activation barriers as listed in Table S3. First, it can be seen that the MM contributions are small and account for less than 6 % of the total ONIOM energies. Second, no quantitative variation trend in activation barriers is found for different transition states. Third, all the MM energy values are almost positive, indicating that the zeolite environment does not have a stabilizing effect on the transition state structures. This remark is consistent with the periodic DFT result for thiophenic derivative cracking over the MOR zeolite reported by Rozanska et al. Their calculations suggests that the zeolite framework appears not to stabilize the transition state complexes [18].

Conclusions

We have performed a two-layer ONIOM study on the HDS mechanism of thiophene in H-FAU and cation-exchanged M-FAU zeolites ($M=Li^+$, Na^+, and K^+). According to the experimental and theoretical studies, we proposed the possible reaction pathways. The calculated results suggest that for the unimolecular HDS mechanism, the rate-determining step is the hydrogenation of alkoxide intermediate. The high activation barriers of C-S bond cracking and desulfurization steps make the unimolecular mechanism unfavorable under moderate conditions. These conclusions are also followed for the unimolecular mechanism of 2-methylthiophene. As compared to the thiophene case, the effect of electron-donating $–CH_3$ group is weak and limited. In addition, the assistance of H_2O and H_2S molecules does not reduce the difficulty of C-S bond cracking more effectively.

Five main steps are involved in the bimolecular cracking mechanism. The rate-determining step is the formation of 2-methylthiophene, not the C-S bond cracking of the thiophene. Furthermore, the ring-opening of thiophene is much easier to occur than the desulfurization step and these two steps are more favorable through bimolecular mechanism. A careful analysis of energetics suggests that H_2S, propene, and methyl thiophene may be the thermodynamically favorable major products for the HDS process of thiophene over H-FAU zeolite, in good agreement with experimental observations. Additionally, we optimized and obtained an alternative to the transition state of desulfurization step of thiophene, whereas the corresponding higher energy barriers disfavor the removal of sulfur atom.

In M-FAU zeolites, desulfurization step could not be completed and no H_2S is produced in the absence of H_2 molecules. The adsorption modes are different from the H-FAU case and the order of adsorption energy is calculated to be $Li^+ > Na^+ > K^+$. For the unimolecular C-S bond cracking step, the metal cations do not reduce the energy barrier effectively as compared to that in H-FAU. More importantly, both bimolecular polymerization and subsequent ring-opening steps of thiophene are favorable in H-FAU, but difficult to occur in M-FAU due to the higher activation barriers (more than 220 kJ/mol), indicating that metal cations increase their difficulty of occurrence. Our conclusions are in accord with experimental observation, i.e., no H_2S is found in Na-MOR and K-LTL zeolites. The removal of thiophene is achieved essentially by physisorption mechanism, not the chemical desulfurization process.

Acknowledgments This work was funded by the National Science Foundation of China (nos. 21203118), the Innovation Program of Shanghai Municipal Education Commission (14YZ147), IIASA Young Scientists Summer Program (21411140044), and the Training Program for Young College Teachers in Shanghai (ZZyyy12005).

References

1. Shan JH, Chen L, Sun LB, Liu XQ (2011) Energ Fuel 25:3093–3099
2. Duan LH, Gao XH, Meng XH, Zhang HT, Wang Q, Qin YC, Zhang XT, Song LJ (2012) J Phys Chem C 116:25748–25756
3. Welters WJJ, Vorbeck G, Zandbergen HW, de Haan JW, de Beer VHJ, van Santen RA (1994) J Catal 150:155–169
4. Hernández-Maldonado AJ, Yang RT (2003) Ind Eng Chem Res 42:123–129
5. Yang RT, Takahashi A, Yang FH (2001) Ind Eng Chem Res 40:6236–6239
6. Chica A, Strohmaier K, Iglesia E (2004) Langmuir 20:10982–10991
7. Richardeau D, Joly G, Canaff C, Magnoux P, Guisnet M, Thomas M, Nicolaos A (2004) Appl Catal A Gen 263:49–61
8. Shan HH, Li CY, Yang CH, Zhao H, Zhao BY, Zhang JF (2002) Catal Today 77:117–126
9. Valla JA, Mouriki E, Lappas AA, Vasalos IA (2007) Catal Today 127:92–98
10. Angelis BA, Appierto G (1975) J Colloid Interface Sci 53:14–19

11. Welters WJJ, de Beer VHJ, van Santen RA (1994) Appl Catal A Gen 119:253–269
12. Yu SY, Li W, Iglesia E (1999) J Catal 187:257–261
13. García CL, Lercher JA (1992) J Phys Chem 96:2669–2675
14. Simon LJ, Rep M, van Ommen JG, Lercher JA (2001) Appl Catal A Gen 218:161–170
15. Hernández-Maldonado AJ, Yang RT (2004) J Am Chem Soc 126: 992–993
16. Saintigny X, van Santen RA, Clemendot S, Hutschka F (1999) J Catal 183:107–118
17. Rozanska X, van Santen RA, Hutschka F (2001) J Catal 200:79–90
18. Rozanska X, van Santen RA, Hutschka F, Hafner J (2003) J Catal 215:20–29
19. Li BR, Guo WP, Yuan SP, Hu J, Wang JG, Jiao HJ (2008) J Catal 253:212–220
20. Nieminen V, Sierka M, Yu Murzin D, Sauer J (2005) J Catal 231: 393–404
21. Namuangruk S, Tantanak D, Limtrakul J (2006) J Mol Catal A Chem 256:113–121
22. Boronat M, Viruela PM, Corma A (2004) J Am Chem Soc 126: 3300–3309
23. Hriljac JA, Eddy MM, Cheetham AK, Donohue JA, Ray GJ (1993) J Solid State Chem 106:66–72
24. Vreven T, Morokuma K, Farkas Ö, Schlegel HB, Frisch MJ (2003) J Comput Chem 24:760–769
25. Vreven TK, Byun S, Komáromi I, Dapprich S, Montgomery JA Jr, Morokuma K, Frisch MJ (2006) J Chem Theory Comput 2: 815–826
26. Zhao Y, Truhlar DG (2008) Theor Chem Acc 120:215–241
27. Rappe AK, Casewit CJ, Colwell KS, Goddard WA III, Skiff WM (1992) J Am Chem Soc 114:10024–10035
28. Becke AD (1993) J Chem Phys 98:5648–5652
29. Namuangruk S, Pantu P, Limtrakul J (2004) J Catal 225:523–530
30. Limtrakul J, Jungsuttiwong S, Khongpracha P (2000) J Mol Struct 525:153–162
31. Heinz H, Suter UW (2004) J Phys Chem B 108:18341–18352
32. Asada N, Fedorov DG, Kitaura K, Nakanishi I, Merz KM Jr (2012) J Phys Chem Lett 3:2604–2610
33. Otsuka M, Tsuchida N, Ikeda Y, Kimura Y, Mutoh Y, Ishii Y, Takano K (2012) J Am Chem Soc 134:17746–17756
34. Frisch MJ, Trucks GW, Schlegel HB, Scuseria GE, Robb MA, Cheeseman JR, Scalmani G, Barone V, Mennucci B, Petersson GA, Nakatsuji H, Caricato M, Li X, Hratchian HP, Izmaylov AF, Bloino J, Zheng G, Sonnenberg JL, Hada M, Ehara M, Toyota K, Fukuda R, Hasegawa J, Ishida M, Nakajima T, Honda Y, Kitao O, Nakai H, Vreven T, Montgomery JA Jr, Peralta JE, Ogliaro F, Bearpark M, Heyd JJ, Brothers E, Kudin KN, Staroverov VN, Kobayashi R, Normand J, Raghavachari K, Rendell A, Burant JC, Iyengar SS, Tomasi J, Cossi M, Rega N, Millam NJ, Klene M, Knox JE, Cross JB, Bakken V, Adamo C, Jaramillo J, Gomperts R, Stratmann RE, Yazyev O, Austin AJ, Cammi R, Pomelli C, Ochterski JW, Martin RL, Morokuma K, Zakrzewski VG, Voth GA, Salvador P, Dannenberg JJ, Dapprich S, Daniels AD, Farkas O, Foresman JB, Ortiz JV, Cioslowski J, Fox DJ (2009) Gaussian 09, Revision A.01. Gaussian, Inc, Wallingford
35. Boys SF, Bernardi F (1970) Mol Phys 19:553–566
36. Garcia CL, Lercher JA (1993) J Mol Struct 293:235–238
37. Murdoch JR (1981) J Chem Educ 58:32–36
38. Sun YX, Yang J, Zhao LF, Dai JX, Sun H (2010) J Phys Chem C 114:5975–5984
39. Bhan A, Joshi YV, Delgass WN, Thomson KT (2003) J Phys Chem B 107:10476–10487
40. Svelle S, Kolboe S, Swang O (2004) J Phys Chem B 108: 2953–2962
41. Correa BJ, Mota CJA (2002) Phys Chem Chem Phys 4:375–380
42. Aksenov DG, Klimov OV, Echevskii GV, Paukshtis EA, Budneva AA (2004) React Kinet Catal Lett 83:187–194
43. Chica A, Strohmaier KG, Iglesia E (2005) Appl Catal B Environ 60:223–232
44. Li Y, Guo WP, Fan WB, Qin ZF, Wang JG (2010) Chin J Catal 31: 1419–1426
45. Geobaldo F, Palomino GT, Bordiga S, Zecchina A, Areán CO (1999) Phys Chem Chem Phys 1:561–569
46. Jaimes L, Tonetto GM, Ferreira ML, Lasa H (2008) Int J Chem React Eng 6:1–65
47. Jaimes L, Ferreira ML, Lasa H (2009) Chem Eng Sci 64: 2539–2561
48. Hosono H, Kawazoe H, Nishii J, Kanazawa T (1982) J Non-Cryst Solids 51:217–240
49. Takahashi A, Yang FH, Yang RT (2002) Ind Eng Chem Res 41: 2487–2496